Experimental Evidence of Radio Frequency Radiation From *Staphylococcus aureus* Biofilms

Menglou Rao, *Graduate Student Member, IEEE*, Kamal Sarabandi, *Life Fellow, IEEE*, John Soukar, Nicholas A. Kotov, and J. Scott VanEpps

***Abstract*—This paper reports the first successful detection of electromagnetic (EM) radiation from *Staphylococcus aureus* biofilms in the gigahertz (GHz) frequency range. Two novel sensing systems are deployed for the measurement. A very sensitive wideband near-zone radiative system specifically designed for this application is first used to search for signals in the 1–50 GHz frequency region. Notable radiation is observed in the 3–4 GHz band. Exposure to lethal doses of Zinc oxide nanopyramids (ZnO-NPY) is used to verify that the signals are indeed produced by living cells rather than material thermal emission. Afterwards, a spiral antenna system is exploited to further examine the band of interest in the near-field region. Radiation from 3 identical biofilm samples is monitored and recorded over 70 days. Two distinct frequency bands, namely the 3.18 GHz and the 3.45 GHz bands, are identified as potential "communication bands". Furthermore, long-term and short-term cycles of the total radiation intensity within the band are observed over the course of the experiment. This work confirms the presence of EM radiation within bacterial communities, which is a key requirement to demonstrate EM signaling among bacterial cells. The insight could lead to breakthroughs in demystifying how cells communicate as well as advancement of important technologies in biology and communication systems.**

***Index Terms*—Biofilms, bacterial, cells, communication, EM signaling, radiation, emission, near-field.**

I. Introduction

ALL biological organisms are complex systems consisting of a large number of interacting elements. They are constantly interchanging information with each other and with the external environment in order to respond/adapt to various conditions. Chemical signaling has been considered the dominant communication mechanism for biological organization and activities, where messages are carried by ligands transmitted by diffusion [1]. However, this type of signaling typically supports communication in the range of hundreds of nanometers, whereas biological systems interact and manifest a certain degree of order even on a macroscopic scale [2]. Since many biomacromolecules and their derivatives are electrically polarized, any oscillations of these structures can generate electromagnetic (EM) fields. The strong electrical polarity of biological objects suggests EM waves may play a role in intra- and inter-cell signaling. There have been extensive postulations of the existence, nature, and function of EM fields in biological systems. H. Fröhlich first proposed the idea that metabolic activities in biological systems may excite coherent electric vibrations, which enable long-range interactions and energy transfer within the system [3]–[5]. This theory builds the foundation for later studies on EM activities in biological cells. The structure that generates EM waves in biological cells has not been identified yet. It has been suggested that microtubules in eukaryotic cells are one of the possible sources [6]–[8]. Microtubules are lattices of oriented dipoles [6]. Theoretical analyses have indicated that the vibrations of microtubules and actin filaments can generate EM fields that mediate the energy transfer with their surroundings. These hypotheses are partly supported by a few experiments [9]–[11]. In [9], the resonance peaks of a single microtubule are identified in the frequency range of 10–30 MHz and 100–200 MHz. In [10], changes of electric field in the frequency range 8-9 MHz are detected in the vicinity of the plasma membrane of yeast mitotic cells in the M phase of the cell cycle, which coincides with the period when the kinetochore microtubules in the mitotic spindle bind chromatids. In [11], it is suggested that possible EM activities in microtubules occur when a low-intensity electric field at 100-300 kHz is applied to mitotic cells. However, none of these experiments have directly detected EM radiation from cells. Other structures such as DNA or proteins are also found to be able to generate EM waves. In [12], it is shown that some bacterial DNA sequences induce EM waves in the kHz range in high aqueous dilutions. In [13], delocalized modes in proteins are identified in the terahertz frequency domain. Nevertheless, these experiments are focused on molecular levels. It is unclear if these EM waves are purposeful signaling or just natural molecular vibrations.

A recent study has indicated that bacterial cells in biofilms may use EM signals to communicate [14]. Biofilms are one

Manuscript received 14 January 2022; revised 1 March 2022 and 26 March 2022; accepted 14 April 2022. Date of publication 9 May 2022; date of current version 23 August 2022. This work was supported by the U.S. Defense Advanced Research Projects Agency (DARPA) RadioBio Program under Contract HR00111720067. *(Corresponding author: Menglou Rao.)*

Menglou Rao and Kamal Sarabandi are with the Radiation Laboratory, Department of Electrical Engineering and Computer Science, University of Michigan, Ann Arbor, MI 48109 USA (e-mail: menglrao@umich.edu; sarabband@umich.edu).

John Soukar is with the Department of Emergency Medicine, Univeristy of Michigan, Ann Arbor, MI 48109 USA (e-mail: soukarjo@umich.edu).

Nicholas A. Kotov is with the Department of Chemical Engineering, Department of Biomedical Engineering, Department of Material Science and Engineering, Department of Macromolecular Science and Engineering, Biointerfaces Institute, University of Michigan, Ann Arbor, MI 48109 USA (e-mail: kotov@umich.edu).

J. Scott VanEpps is with the Department of Emergency Medicine, Department of Biomedical Engineering, Macromolecular Science and Engineering, Biointerfaces Institute, Weil Institute for Critical Care Research and Innovation, University of Michigan, Ann Arbor, MI 48109 USA (e-mail: jvane@med.umich.edu).

Digital Object Identifier 10.1109/JERM.2022.3168618

2469-7249 © 2022 IEEE. Personal use is permitted, but republication/redistribution requires IEEE permission.
See https://www.ieee.org/publications/rights/index.html for more information.

Authorized licensed use limited to: The University of British Columbia Library. Downloaded on October 11,2026 at 00:43:51 UTC from IEEE Xplore. Restrictions apply.

of the most ubiquitous forms of biological systems on earth, and are commonly associated with infectious diseases [15]. They are also responsible for contamination of medical devices and implants [16], deterioration of water quality [17], and microbial induced corrosion [18]. Further understanding of communication mechanisms within biofilm communities is of great importance to effective biofilm control and management.

Biofilms are essentially aggregates of microorganisms in which cells are embedded in a self-produced matrix of extracellular polymeric substances (EPS) [19]. Within the EPS of specific types of biofilms (*e.g.*, *Staphylococcus aureus*, and *Bacillus subtilis*), there are biological elements called amyloid fibrils which are basically characterized as elastic helical fibers with permanent dipole charges at their ends [20]–[22]. [14] postulates that these charged amyloid fibrils can act as mechanical antennas and may be responsible for purposeful signaling among cells in biofilms. A multi-physics model based on an electromagnetically coupled system of mechanical oscillators is developed to characterize the EM signals generated in *S. aureus* biofilms. The model predicts that possible EM radiation could occur within the kHz-GHz frequency range, depending on the mechanical properties of the cells and the amyloid fibrils. [23] compares EM signaling with quorum sensing. It is demonstrated that EM signaling can provide a substantially higher data rate over a much longer range while requiring far less energy than quorum sensing. Therefore, EM signaling may be the preferred method of communication used by cells in biofilms. However, there is no experimental evidence to support EM communications within biofilms so far.

This work is an experimental study designed to complement the theoretical study in [14]. We aim to explore the existence of the predicted EM signals in *S. aureus* biofilms. Based on the theoretical model, we divided the potential radiating frequencies into three groups, i.e., low frequency range (below 1 MHz), MHz range (1 MHz–1 GHz) and GHz range (1–50 GHz), and developed several measurement systems to examine each group individually. Measurements above 50 GHz have not been attempted yet. This paper reports the measurements conducted in the GHz range. A wideband near-zone radiative system [24] is first used to search for possible radiation in the frequency spectrum from 1 to 50 GHz. The frequency range is later narrowed down to 3–20 GHz. We observe notable EM radiation activity in the 3–4 GHz frequency band multiple times on different biofilm samples. In the 3–4 GHz band, we conduct a 70-day longitudinal measurement on a group of 3 identical *S. aureus* biofilm samples using a spiral antenna system. The measurement is performed at a closer range with much finer spectral resolution. Over the course of the measurement, the radiation from all biofilm samples exhibits similar short- and long-term time cycles. The average power density generated by the biofilms is also calculated based on the measured power spectrum. This is the first time that GHz EM radiation from bacterial biofilms has been observed and characterized. The successful detection of such radiation verifies the theoretical model and represents substantial progress in understanding the mechanisms of EM signaling among cells in biofilms. Correlation studies between EM radiation signals and cell gene expression and biofilm morphology are currently in progress, and will be reported in the future.

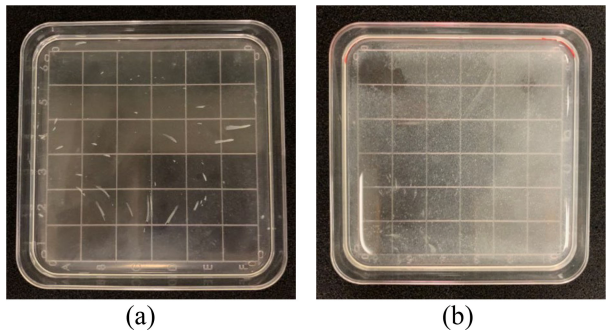


Fig. 1. (a) An 8-day-old sample and (b) a 28-day-old sample in a 100mm × 100mm polystyrene square petri dish.

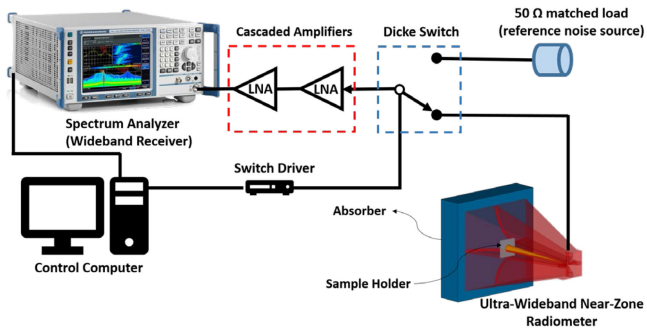


Fig. 2. Diagram of the wideband near-zone radiative system.

II. Measurement of EM Radiation Using the Wideband Near-Zone Radiative System

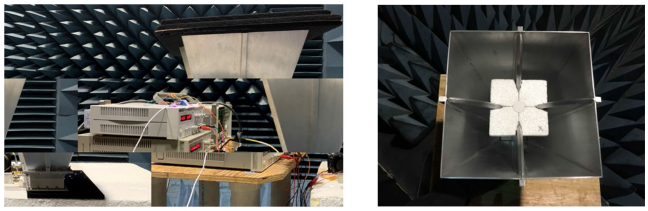
A. Sample Preparation

Methicillin-resistant *S. aureus* substrain USA300 was used in all experiments. A glycerol stock of the strain was maintained at −80 °C and was plated on tryptic soy agar. Single colony inoculates were grown overnight in peptone-NaCl-glucose media (PNG) under shaking conditions at 37 °C. PNG is reported to induce formation of amyloid fibers [25]. Overnight cultures were then diluted 1:10 into fresh PNG and added to a 100 mm × 100 mm polystyrene square petri dish for a final volume of 20 ml and a final concentration of 2×10^5 CFU/ml. These samples were left to grow under static conditions at 37 °C to facilitate biofilm formation. On the day of each measurement, the media were carefully removed and replaced with 10 ml fresh PNG media prior to beginning the measurement. Biofilms were maintained in this manner for the entire duration of the experiment. Fig. 1(a) and (b) show an 8-day-old and a 28-day-old sample, respectively. A set of three 10 ml fresh PNG media samples, without biofilms, are prepared in the same manner as a control group.

B. Measurement Setup and System Characterization

Wideband measurements from 1–50 GHz were first conducted using a specially designed wideband near-zone radiative system [24]. The system consists of a wideband dual-polarized

Authorized licensed use limited to: The University of British Columbia Library. Downloaded on October 11,2026 at 00:43:51 UTC from IEEE Xplore. Restrictions apply.



(a) (b)

Fig. 3. (a)The wideband near-zone radiative system and (b) the zoom-in view of the inside of the signal collector in an anechoic chamber.

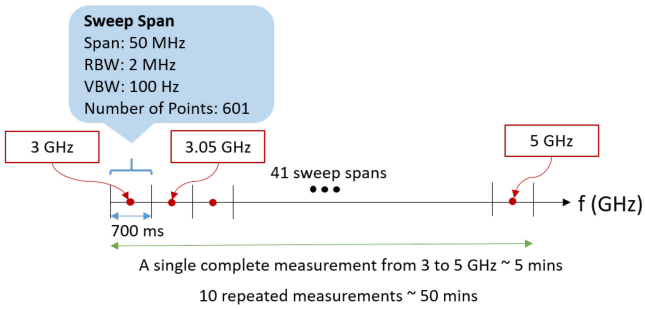


Fig. 4. The data acquisition process for the 3–5 GHz frequency group. A single complete measurement from 3–5 GHz takes about 5 minutes. 10 repeated measurements take about 50 minutes.

signal collector, a Dicke switch [26], two broadband low-noise amplifiers, and a precision spectrum analyzer. Fig. 2 illustrates the system diagram. The signals received by the collector are first fed into one port of the Dicke switch, then amplified by the cascaded amplifiers and recorded by the spectrum analyzer. The amplifiers are placed as close to the output of the signal collector as possible to improve the signal to noise ratio (SNR). The Dicke switch is basically a single-pole-double-throw (SPDT) switch used to calibrate the gain fluctuations of the amplifiers. The other port of the switch is terminated with a 50 Ω matched load at a constant temperature which serves as a reference noise source. The switch alternates between the signal collector and the matched load. The sweep frequency of the spectrum analyzer is synchronized with the switching frequency, therefore, during two consecutive sweeps, the data are first collected from the signal collector, and then from the matched load. If the sweep time of the spectrum analyzer is short enough (on the order of millisecond), the gain of the amplifier can be assumed constant during two consecutive sweeps, and the gain variations of the amplifiers can be eliminated by normalizing the power measured from the signal collector to that from the matched load.

Fig. 3(a) and (b) show the experiment setup in the anechoic chamber at the University of Michigan and the zoomed-in view of the inside of the signal collector, respectively. During the measurement, the biofilm sample is situated at the focal point on the aperture of the signal collector. The measurements are conducted in the anechoic chamber to prevent possible external interference.

The sensitivity of the system is determined by both the specifications of individual components (i.e., noise figure, gain/insertion loss, etc.) and the settings of the spectrum analyzer (i.e., the sweep time, resolution bandwidth, bandwidth, etc.). Based on the system characterization reported in [24], the system is able to detect signals as weak as -191 dBm/Hz.

III. Data Acquisition and Analysis

The system is controlled by a computer through an automated data collection program. The measurement was first conducted from 1–50 GHz. Since there was no indication of any EM radiation above 20 GHz, we restricted our focus on the lower portion of the GHz spectrum. To further improve the sensitivity of the system, we replaced the two broadband low-noise amplifiers with an ultra-low-noise amplifier (3–20 GHz) cascaded with a high-gain amplifier (0.8–21 GHz). For measurements from 3–20 GHz, the entire frequency span was partitioned into four frequency groups, specifically 3–5 GHz, 5–10 GHz, 10–15 GHz and 15–20 GHz, which were examined individually. Each frequency group is further divided into small "sweep spans". For each sweep span, the system takes a sweep and records the average value of 601 data points. If the measurements are repeated multiple times, the results are then averaged among all the measurements. Fig. 4 illustrates the data acquisition process for the 3–5 GHz frequency group. The choices of the sweep span, resolution bandwidth, video bandwidth and the number of repeated measurements directly affect the measurement time and accuracy. We have experimented with different settings and carefully evaluated the tradeoff between the measurement time and accuracy. The final settings are listed in Table I. For these settings, a single complete measurement from 3–5 GHz takes about 5 minutes. The measurement is repeated 10 times, which take a total of 50 minutes. For the other three frequency groups, each takes 125 minutes to complete 10 repeated measurements.

TABLE I
Near-Zone Radiative System Spectrum Analyzer Settings

Span	50 MHz
Resolution Bandwidth (RBW)	2 MHz
Video Bandwidth (VBW)	100 Hz
Sweep Time	700 ms
Number of Repetitions	10

The measurement is first performed on the biofilm samples, and then performed on the fresh PNG samples (control group). The power received from the biofilm sample is compared with that from the PNG sample by taking the ratio of the two measurements

$$R_{\text{sample}} = \frac{P_{\text{biofilm}}}{P_{\text{PNG}}} \tag{1}$$

In this way, any background noise and systematic errors can be effectively removed. A baseline is established by taking the ratio of two PNG measurements

$$R_{\text{baseline}} = \frac{P_{\text{PNG},2}}{P_{\text{PNG},1}} \tag{2}$$

The fluctuations between two PNG measurements (baseline) are less than ±0.05 dB within the entire frequency range, indicating that any frequencies where $R_{\text{sample}} > 0.05$ dB are considered possible "communication bands". The flowchart of the algorithm and main MATLAB code for processing the data can

Authorized licensed use limited to: The University of British Columbia Library. Downloaded on October 11,2026 at 00:43:51 UTC from IEEE Xplore. Restrictions apply.

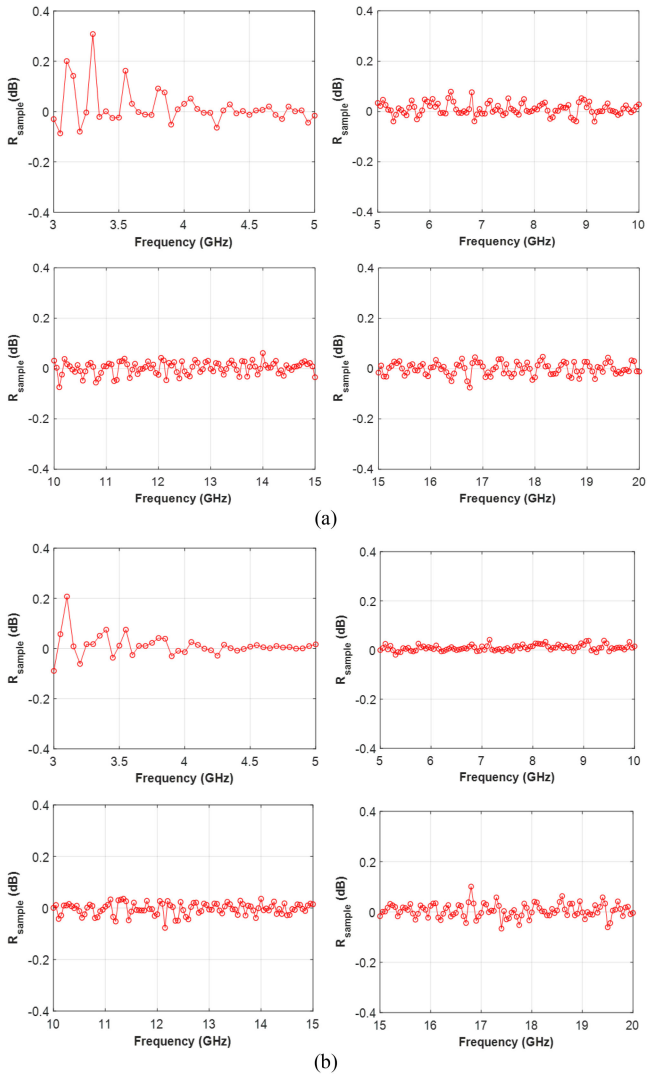


Fig. 5. Measurement results from (a) a 43-day-old biofilm sample. Sample birth date: September 17th, 2019. Measurement date: October 30th, 2019, and from (b) a 20-day-old biofilm sample. Sample birth date: October 18th, 2019. Measurement date: November 7th, 2019.

be found in Appendix. Fig. 5(a) and (b) show the results obtained from a 43-day-old and a 20-day-old biofilm samples, respectively, using the settings listed in Table I. The power received from the biofilm sample is notably higher than that from the PNG sample in the 3–4 GHz frequency band whereas no significant differences between the sample and the control are measured at other frequencies. It should be noted that the measurement was repeated 3–4 times every day (excluding weekends) from June 2019 to December 2019, and was performed on a large number of samples of different ages. Similar frequency responses were observed repeatedly.

IV. ZnO-NPY Exposure Experiments on Biofilm Samples

The validity of a biological source of the radiation in the 3–4 GHz range was examined by exposing biofilms samples to ZnO nanopyramids (ZnO-NPY). ZnO nanopyramids with hexagonal base (ZnO-NPYs) are synthesized nanoparticles that have been characterized extensively [27]–[29]. It has been previously demonstrated that ZnO-NPYs have strong antibacterial effects on *S. aureus*. They disrupt cell membranes and metabolism, leading to cell death without destroying the structure of the biofilms. For the ZnO-NPY exposure experiment, dry ZnO-NPY powder was measured and reconstituted into PNG media and sonicated for 5 minutes to ensure dispersion. Concentrations of ZnO-NPYs were made at 500 μg/ml to ensure lethality [28].

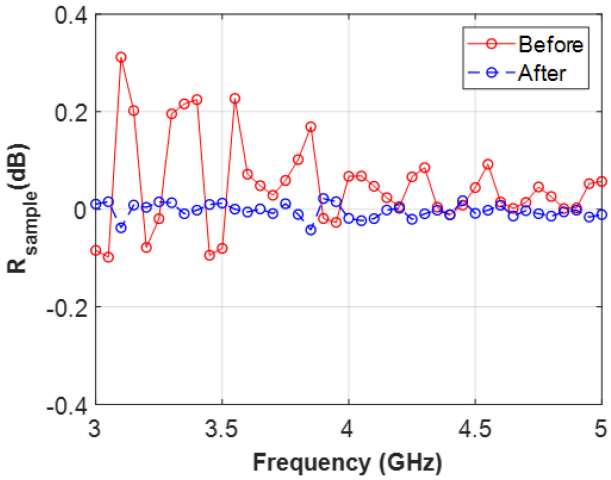


Fig. 6. Frequency responses of a 30-day-old biofilm sample before and after the ZnO-NPY treatment. Sample birth date: November 12, 2019. Measurement date: December 4, 2019.

We first measured the biofilm sample following the procedure described in Sections II and III, then we added 10 ml ZnO-NPY to both the biofilm sample and the PNG control sample, and took the measurement again. Fig. 6 shows the frequency responses of a 30-day-old biofilm sample before and after the ZnO-NPY treatment. As observed previously, the biofilm sample exhibits strong radiation in the 3-4 GHz band in its natural state. After the ZnO-NPY treatment, the frequency response becomes relatively flat over the band of interest, indicating that the signal is indeed generated by the metabolic activities of the living constituent cells rather than thermal emission of the biofilm material.

V. Monitoring Signal Timescales Using the Spiral Antenna System

The previous experiments prove the existence of EM radiation from living *S. aureus* biofilms, however, they do not provide further information about the biological functions of such a signal. Knowing the timescales of the signal can help relate EM radiation to key biological activities, therefore, a rigorously controlled 70-day longitudinal experiment is conducted to monitor the signal intensity of 3 identical biofilm samples. Based on the prior results, we now only focus on the 3–3.6 GHz frequency range.

A spiral antenna system operating from 2–8 GHz with a short far-field distance is chosen for this experiment. The new system is a slightly modified version of the wideband near-zone radiative

Authorized licensed use limited to: The University of British Columbia Library. Downloaded on October 11,2026 at 00:43:51 UTC from IEEE Xplore. Restrictions apply.

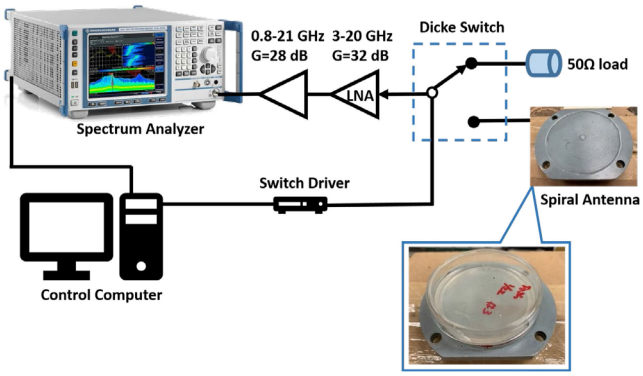


Fig. 7. The spiral antenna system diagram with a close-up view of a biofilm sample on the spiral antenna.

TABLE II
SPIRAL ANTENNA SYSTEM SPECTRUM ANALYZER SETTINGS

Span	20 MHz
Resolution Bandwidth (RBW)	2 MHz
Video Bandwidth (VBW)	100 Hz
Sweep Time	500 ms
Number of Repetitions	10

system, where the signal collector is replaced by a spiral antenna. Fig. 7 shows the system diagram.

The preparation of biofilm samples follows the same procedure described in Section II, Part A. For the new system, the culture was diluted 1:10 into PNG and inoculated into a circular polystyrene petri dish with a diameter of 60 mm for a total final volume of 10 ml and a final concentration of 2×10^5 CFU/ml. The size of the petri dish is chosen such that the biofilms can cover the entire aperture of the spiral antenna. During the measurement, the petri dish is directly placed on top of the spiral antenna as shown in the close-up view in Fig. 7.

For data acquisition, a smaller span is chosen to achieve a shorter sweep time. The spectrum analyzer settings are listed in Table II. The new system features less propagation path-loss and higher sensitivity. The fluctuations of the baseline are less than ± 0.03 dB.

We grew 3 biofilm samples on July 13, 2020, and the measurements were conducted from July 16, 2020 (Day 3) through September 21, 2020 (Day 70). The measurements started at the same time on each day to eliminate the possibility of signal fluctuation throughout the day. Fig. 8(a)–(h) show the frequency responses of Sample # 3 on July 20th (Day 7), July 23rd (Day 10), July 30th (Day 17), August 4th (Day 22), August 6th (Day 24), August 12th (Day 30), September 2nd (Day 51), and September 18th (Day 67), respectively. R_{sample} and R_{baseline} are given by (1) and (2), respectively. Two photos of the sample taken on Day 7 and Day 30 are presented in Fig. 8(a) and (f). Two distinct communication bands are identified, which are the 3.15–3.2 GHz band and the 3.4–3.5 GHz band. The frequency responses of these biofilm samples are comparable to those observed using the wideband near-zone radiative system. The slight frequency shift could be resulted from the variations in the shape and size of the biofilm constituents. The smaller petri dish concentrates

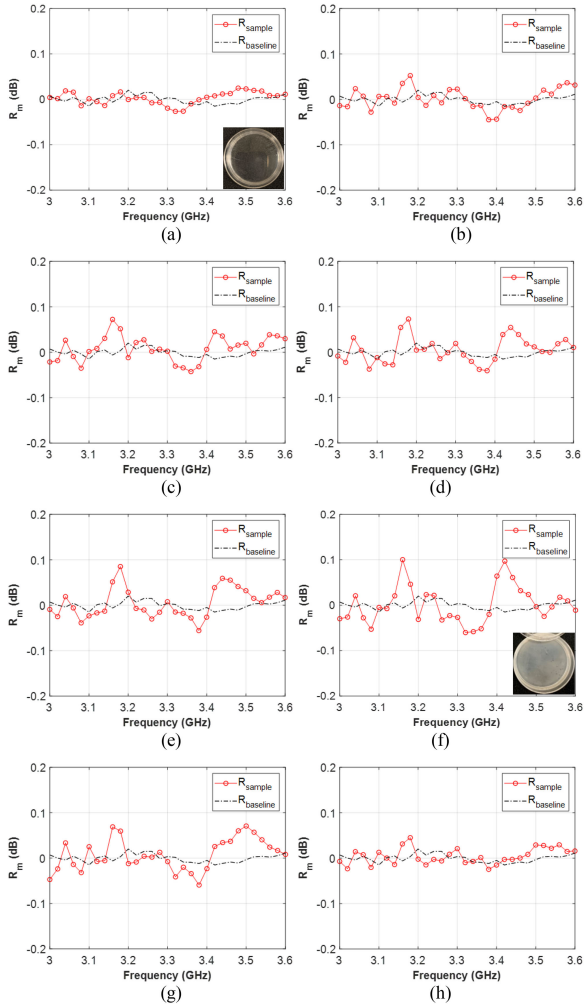


Fig. 8. Frequency responses of biofilm sample #3 on (a) July 20th (Day 7), (b) July 23rd (Day 10), (c) July 30th (Day 17), (d) August 4th (Day 22), (e) August 6th (Day 24), (f) August 12th (Day 30), (g) September 2nd (Day 51), and (h) September 18th (Day 67).

the inoculum over a smaller area, accelerating the initial biofilm forming process and may change the ultimate structure. Based on the multi-physics model, the frequency of the radiation directly depends on the dimensions of the cells and the amyloid fibrils. Moreover, since there is less total biomass in a small petri dish, the maximum amplitude of the signal is expected to be smaller than that measured from a large petri dish. Fig. 9(a) and (b) show the power spectrum density (PSD) of the biofilm sample and the PNG, in the 3.15–3.2 GHz band and the 3.4–3.5 GHz band, respectively. The results were obtained from the measurements conducted on August 12th, when the strongest radiation was observed. At first glance, the measured PSD of the biofilm sample is only about 0.2 dB above the measured PSD of the background noise. This difference may seem too small to claim signal detection. However, the following analysis clearly demonstrates that the 0.2 dB difference is actually a very large dynamic range and is strong evidence of the existence of EM radiation from biofilms.

Authorized licensed use limited to: The University of British Columbia Library. Downloaded on October 11,2026 at 00:43:51 UTC from IEEE Xplore. Restrictions apply.

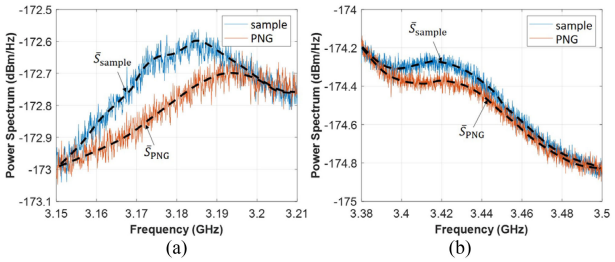


Fig. 9. Power spectrum density of the biofilm sample and PNG in the (a) 3.15–3.2 GHz and (b) 3.4–3.5 GHz bands.

First, it should be emphasized that Fig. 9 is just a sample of many measurements that we have taken. Our detection criteria are based on the average (mean) values of the measured PSDs of the biofilm samples ($\bar{S}_{\text{sample}}$) and background noise ($\bar{S}_{\text{PNG}}$).

The PSD of the background noise S_{PNG} is a Gaussian process with a probability density function [26]

$$f\ (S_{\text{PNG}}) = \frac{1}{\Delta S\sqrt{2\pi}}\ e^{-\frac{1}{2}\left(\frac{S_{\text{PNG}}-\bar{S}_{\text{PNG}}}{\Delta S}\right)^2} \tag{3}$$

where $\bar{S}_{\text{PNG}}$ is the average noise PSD and ΔS is the standard deviation (also known as measurement uncertainty). The measured PSD with 95% confidence is within

$$S_{\text{PNG}} = \bar{S}_{\text{PNG}}\ \pm 1.96\Delta S \tag{4}$$

The measurement accuracy is dictated by ΔS, which is related to the resolution bandwidth (RBW) and video bandwidth (VBW) of the spectrum analyzer, and the number of repeated measurements *(N)* used in estimating the average PSD [24]

$$\Delta S\ = \frac{\bar{S}_{\text{PNG}}}{\sqrt{N\frac{\text{RBW}}{\text{VBW}}}} \tag{5}$$

(5) indicates that we can reduce the uncertainty of the measurement by increasing the ratio between RBW and VBW, and by averaging over many repeated measurements. In our case, RBW = 2 MHz, VBW = 100 Hz and $N = 10$.

Referring to Fig. 9(a) as an example, for average background noise of $\bar{S}_{\text{PNG}} = -172.8$ dBm/Hz (5.2481×10^{-18}mW/Hz), the standard deviation of the measured noise PSD is

$$\Delta S\ = \frac{5.2481 \times 10^{-18}}{\sqrt{10 \times \frac{2\times 10^6}{100}}}\ =\ 1.1735 \times 10^{-20}\ \text{mW/Hz}$$

The 95% confidence interval of the measured background noise is $(5.2481 \times 10^{-18} \pm 2.3001 \times 10^{-20})$ mW/Hz or (-172.8 ± 0.019) dBm/Hz in logarithmic scale. The estimated mean of the signal measured from the biofilm sample is -172.65 dBm/Hz (5.4325×10^{-18} mW/Hz), therefore, the average PSD generated by the biofilms is

$$\bar{S}_{\text{bio}} = \bar{S}_{\text{sample}}\ -\ \bar{S}_{\text{PNG}} =\ 1.8443 \times 10^{-19}\ \text{mW/Hz}$$

This is 15.7 standard deviation away from the mean of the noise. In signal detection, the probability of false detection for a given threshold T (i.e., when noise exceeds the threshold T) is given by [30]

$$P_r\ (S \geq T) = \int_T^{\infty} f\ (S)\ dS\ = \frac{1}{2}\left[1 - \text{erf}\left(\frac{T-\bar{S}}{\Delta S\sqrt{2}}\right)\right] \tag{6}$$

in which $f(S)$ is the probability density function of the background noise given by (3) and erf$(\cdot)$ is the error function. Table III lists the probability of false detection for different threshold values. Typically, the detection threshold is set to 2 – 3 standard deviation away from the mean of the noise. For a signal that is more than 15 standard deviation away from the mean value of the background noise, the chance of it being noise is almost zero. Therefore, it is unquestionable that the measured signals are radiation generated by the biofilms.

TABLE III
PROBABILITY OF FALSE DETECTION FOR DIFFERENT THRESHOLD VALUES ($T = \bar{S} + n\Delta S$)

n	1	2	3	**15**
P(false detection) %	15.8655	2.2750	0.1350	$\mathbf{3.6710 \times 10^{-49}}$

TABLE IV
KEY PARAMETERS OF THE RADIATED SIGNAL

	3.15-3.2 GHz Band	**3.4-3.5 GHz bands**
f_1	3.15	3.193
f_2	3.405	3.459
P	-112.5 dBm	-114.5 dBm
P_v	-122.5 dBm/mm^3	-124.5 dBm/mm^3

* Average thickness $t = 3.5$ um is used to calculate P_v

Based on the power spectrum, we can also estimate the maximum total radiated power from the biofilms using

$$P\ = \int_{f_1}^{f_2} (S_{\text{sample}} - S_{\text{PNG}})\ df \tag{7}$$

where f_1 and f_2 are the lower and higher ends of the spectrum where the sample line is above the PNG line. The power density generated by the biofilms can be estimated from

$$P_v = \frac{P}{\pi r^2 t} \tag{8}$$

where $r = 30$ mm is the radius of the petri dish and t is the thickness of the biofilms. The thickness of the biofilms used in the experiments is in the range of 2–5 um. We use the average thickness $t = 3.5$ um in the calculations. Table IV summarizes the key parameters of the observed radiation. Although only the frequency responses of Sample #3 are presented in Figs. 8 and 9, it should be noted that similar phenomena are also observed in the other two samples.

The series of frequency responses shown in Fig. 8 present the detailed frequency spectrum of the biofilm sample on each day, however, it is difficult to evaluate how the signal evolves over time based on individual frequency responses. To quantitatively describe the radiation intensity across the entire frequency band and demonstrate the variation of the signal over time, a parameter Δ defined by:

$$\Delta\ = \sum_{i=1}^{n} |R_{\text{sample}}\ (i)|\ -\ \sum_{i\ =\ 1}^{n} |R_{\text{baseline}}\ (i)| \tag{9}$$

Authorized licensed use limited to: The University of British Columbia Library. Downloaded on October 11,2026 at 00:43:51 UTC from IEEE Xplore. Restrictions apply.

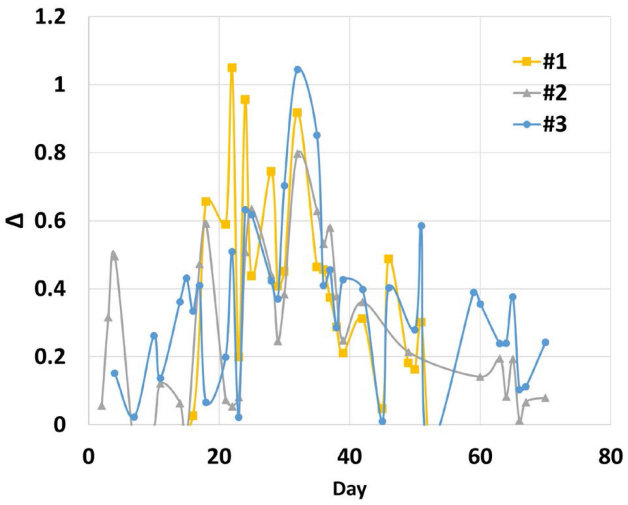


Fig. 10. The radiation strength (Δ) of the 3 biofilm samples from Day 3 to Day 70.

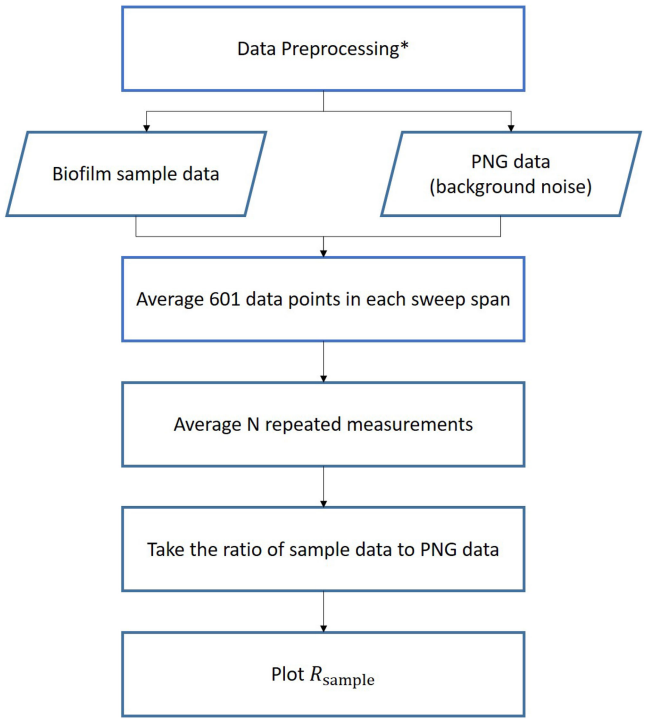
is introduced, where n is the number data points in the frequency response plot. Fig. 10 shows Δ for each sample over the 70-day timescale. The radiation from Samples #2 and #3 exhibit similar long-term patterns: the radiation intensity increases gradually and reaches the maximum around day 32. After that, the radiation intensity gradually decreases. Sample #1 also exhibits significant radiation on day 32, but has two other radiation peaks on day 22 and day 24. In addition to the long-term pattern, several short-term fluctuations ranging from 1-5 days are also observed. The significance of these timeframes is still under investigation. One way to explain this behavior is by noting the presence of multiple harmonics with respect to the biofilm life cycles which depend on nutrients, temperature, strain, etc [31]. This phenomenon is quite similar to the dynamics of quorum sensing in biofilms [32]–[34].

VI. Conclusion

Although it has long been suggested that biological cells may transmit and receive EM waves, no prior convincing experimental evidence has been generated to support this hypothesis prior to this paper. Our work is the first successful attempt to measure EM radiation from *S. aureus* biofilms in the GHz frequency range. Two measurement systems are used in the experiments. Two distinct radiating bands in the 3-4 GHz frequency range are identified. Over the course of a 70-day experiment, we discovered a long-term cycle of the radiated signal with short-term fluctuations. This work proves the existence of EM radiation in biofilm communities, which is validated by examining multiple samples over a long period of time and comparing the measured power with that of PNG media (no biofilms) in the same petri dish. In addition, it is shown that exposing biofilms with significant RF radiation to lethal doses of ZnO-NPYs, which inhibits metabolic activity, eliminates the biofilm RF emission.

Appendix

Flowchart of the data processing algorithm



*In data preprocessing, all data are normalized to the matched load to calibrate the gain variation of the amplifier. The data are configured into 3D datasets with dimensions of $601 \times m \times N$, where m is the number of sweep spans and N is the number of repeated measurements used for average.

Main MATLAB code

```
% 1.average measured power in each sweep span
sample_avgSpan = mean(sample_data,1);
PNG_avgSpan = mean(PNG_data,1);
% 2.average N repeated measurements
sample_avgTrace = mean(sample_avgSpan,3);
PNG_avgTrace = mean(PNG_avgSpan,3);
% 3.take the ratio of sample to media
ratio_avgFinal = sample_avgTrace./PNG_avgTrace;
```

**All data are in linear scale.

Acknowledgment

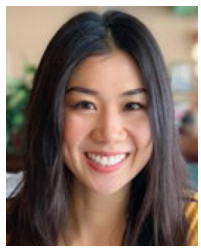
This work was supported by the U.S. Defense Advanced Research Projects Agency (DARPA) RadioBio program under contract HR00111720067.

References

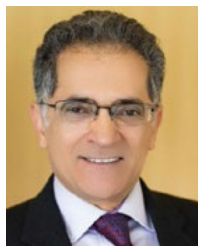
[1] C. Rye, W. Robert, V. Jurukovski, J. DeSaix, C. Jung, and Y. Avissar, "Cell communication," in *Proc. Biology*, Houston, TX, USA: OpenStax, 2016, pp. 247–264.
[2] B. Alberts *et al.*, *Molecular Biology of the Cel*. 6th ed. New York, NY, USA: Garland Science, 2014.
[3] H. Fröhlich and F. Kremer, *Coherent Excitations in Biological Systems*. Berlin, Heidelberg: Springer Berlin Heidelberg, 1983, vol. 53, no. 9.

Authorized licensed use limited to: The University of British Columbia Library. Downloaded on October 11,2026 at 00:43:51 UTC from IEEE Xplore. Restrictions apply.

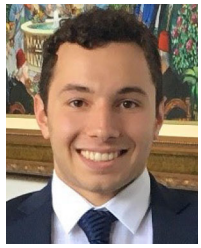
[4] H. Fröhlich, *Biological Coherence and Response to External Stimuli*. Berlin, Heidelberg: Springer Berlin Heidelberg, 1988.
[5] H. Fröhlich, "The biological effects of microwaves and related questions," *Adv. Electron. Electron Phys.*, vol. 53, pp. 85–152, 1980.
[6] J. A. Tuszyński, S. Hameroff, M. V. Satarić, B. Trpisová, and M. L. A. Nip, "Ferroelectric behavior in microtubule dipole lattices: Implications for information processing, signaling and assembly/disassembly," *J. Theor. Biol.*, vol. 174, no. 4, pp. 371–380, 1995.
[7] J. Pokorný, F. Jelínek, V. Trkal, I. Lamprecht, and R. Hölzel, "Vibrations in microtubules," *J. Biol. Phys.*, vol. 23, no. 3, pp. 171–179, 1997.
[8] M. Cifra, J. Pokorný, D. Havelka, and O. Kučera, "Electric field generated by axial longitudinal vibration modes of microtubule," *BioSystems*, vol. 100, no. 2, pp. 122–131, 2010.
[9] S. Sahu *et al.*, "Atomic water channel controlling remarkable properties of a single brain microtubule: Correlating single protein to its supramolecular assembly," *Biosens. Bioelectron.*, vol. 47, pp. 141–148, 2013.
[10] J. Pokorný, J. Hašek, F. Jelínek, J. Šaroch, and B. Palán, "Electromagnetic activity of yeast cells in the M phase," *Electromagn. Biol. Med.*, vol. 20, no. 3, pp. 371–396, 2001.
[11] E. D. Kirson *et al.*, "Disruption of cancer cell replication by alternating electric fields," *Cancer Res.*, vol. 64, no. 9, pp. 3288–3295, 2004.
[12] L. Montagnier, J. Aïssa, S. Ferris, J. L. Montagnier, and C. Lavalléee, "Electromagnetic signals are produced by aqueous nanostructures derived from bacterial DNA sequences," *Interdiscip. Sci. Comput. Life Sci.*, vol. 1, no. 2, pp. 81–90, 2009.
[13] D. A. Turton, H. M. Senn, T. Harwood, A. J. Lapthorn, E. M. Ellis, and K. Wynne, "Terahertz underdamped vibrational motion governs protein-ligand binding in solution," *Nat. Commun.*, vol. 5, pp. 2–7, 2014.
[14] N. Barani and K. Sarabandi, "Theory of electromagnetic-based communication within bacterial communities," in *Proc. IEEE Int. Symp. Antennas Propag. Usn. Radio Sci. Meet. APSURSI*, 2019, pp. 353–354.
[15] J. W. Costerton *et al.*, "Bacterial biofilms in nature and disease," *Annu. Rev. Microbiol.*, vol. 41, no. 1, pp. 435–464, Oct. 1987.
[16] A. K. Deva, W. P. Adams, and K. Vickery, "The Role of Bacterial Biofilms in Device-Associated Infection," *Plast. Reconstr. Surg.*, vol. 132, no. 5, pp. 1319–1328, Nov. 2013.
[17] J. Wingender and H.-C. Flemming, "Biofilms in drinking water and their role as reservoir for pathogens," *Int. J. Hyg. Environ. Health*, vol. 214, no. 6, pp. 417–423, Nov. 2011.
[18] B. J. Little and J. S. Lee, "Microbiologically influenced corrosion: An update," *Int. Mater. Rev.*, vol. 59, no. 7, pp. 384–393, Sep. 2014.
[19] Y. Wu, J. Liang, K. Rensing, T.-M. Chou, and M. Libera, "Extracellular matrix reorganization during cryo preparation for scanning electron microscope imaging of Staphylococcus aureus biofilms," *Microsc. Microanal.*, vol. 20, no. 5, pp. 1348–1355, Oct. 2014.
[20] N. Van Gerven, S. E. Van der Verren, D. M. Reiter, and H. Remaut, "The role of functional amyloids in bacterial virulence," *J. Mol. Biol.*, vol. 430, no. 20, pp. 3657–3684, 2018.
[21] G. Yoon, J. Kwak, J. I. Kim, S. Na, and K. Eom, "Mechanical characterization of amyloid fibrils using coarse-grained normal mode analysis," *Adv. Funct. Mater.*, vol. 21, no. 18, pp. 3454–3463, 2011.
[22] S. S. Rogers, P. Venema, J. P. M. van der Ploeg, E. van der Linden, L. M. C. Sagis, and A. M. Donald, "Investigating the permanent electric dipole moment of β-lactoglobulin fibrils, using transient electric birefringence," *Biopolymers*, vol. 82, no. 3, pp. 241–252, Jun. 2006.
[23] N. Barani and K. Sarabandi, "Signaling and quorum sensing within biofilms: Which mechanism is the most probable means of communication?," in *Proc. Annu. Int. Conf. IEEE Eng. Med. Biol. Soc. EMBS*, 2020, pp. 2459–2462.
[24] S. M. Amjadi, M. Rao, and K. Sarabandi, "Wideband near-zone radiative system for exploring the existence of electromagnetic emission from biological samples," *IEEE Trans. Instrum. Meas.*, vol. 69, no. 10, pp. 8344–8351, Oct. 2020.
[25] K. Schwartz, A. K. Syed, R. E. Stephenson, A. H. Rickard, and B. R. Boles, "Functional amyloids composed of phenol soluble modulins stabilize Staphylococcus aureus biofilms," *PLoS Pathog.*, vol. 8, no. 6, Jun. 2012, Art. no. e1002744.
[26] F. Ulaby and D. Long, *Microwave Radar and Radiometric Remote Sensing*. Ann Arbor, MI, USA: The Univ. of Michigan Press, 2014.
[27] M. Yang, K. Sun, and N. A. Kotov, "Formation and assembly–Disassembly processes of ZnO hexagonal pyramids driven by dipolar and excluded volume interactions," *J. Am. Chem. Soc.*, vol. 132, no. 6, pp. 1860–1872, Feb. 2010.
[28] M. J. McGuffie *et al.*, "Zinc oxide nanoparticle suspensions and layer-by-layer coatings inhibit staphylococcal growth," *Nanomedicine Nanotechnol., Biol. Med.*, vol. 12, no. 1, pp. 33–42, Jan. 2016.
[29] U. Kadiyala, E. S. Turali-Emre, J. H. Bahng, N. A. Kotov, and J. S. VanEpps, "Unexpected insights into antibacterial activity of zinc oxide nanoparticles against methicillin resistant Staphylococcus aureus (MRSA)," *Nanoscale*, vol. 10, no. 10, pp. 4927–4939, 2018.
[30] R. N. McDonough and A. D. Whalen, *Detection of Signals in Noise*. 2nd ed. San Diego, CA, USA: Academic, 1995.
[31] S. Periasamy *et al.*, "How Staphylococcus aureus biofilms develop their characteristic structure," *Proc. Natl. Acad. Sci. USA*, vol. 109, no. 4, pp. 1281–1286, Jan. 2012.
[32] J. Pérez-Velázquez, M. Gölgeli, and R. García-Contreras, "Mathematical modelling of bacterial quorum sensing: A review," *Bull. Math. Biol.*, vol. 78, no. 8, pp. 1585–1639, Aug. 2016.
[33] M. Marenda, M. Zanardo, A. Trovato, F. Seno, and A. Squartini, "Modeling quorum sensing trade-offs between bacterial cell density and system extension from open boundaries," *Sci. Rep.*, vol. 6, no. 1, Dec. 2016, Art. no. 39142.
[34] J. M. Yarwood, D. J. Bartels, E. M. Volper, and E. P. Greenberg, "Quorum sensing in Staphylococcus aureus biofilms," *J. Bacteriol.*, vol. 186, no. 6, pp. 1838–1850, Mar. 2004.



Menglou Rao (Graduate Student Member, IEEE) received the B.Eng. degree in electrical engineering from the Beijing University of Posts and Telecommunications, Beijing, China, in 2016. She is currently working toward the Ph.D. degree in electrical and computer engineering from the University of Michigan, Ann Arbor, MI, USA. Since 2017, she has been a Graduate Research Assistant with the Radiation Laboratory, Department of Electrical Engineering and Computer Science, University of Michigan. Her research interests include miniaturized antennas, mm-wave antenna design, and measurements.



Kamal Sarabandi (Life Fellow, IEEE) is currently the Rufus S. Teesdale Endowed Professor of engineering with the University of Michigan, Ann Arbor, MI, USA. He has authored or coauthored many book chapters, more than 315 papers in refereed journals, and more than 760 conference papers. His research interests include microwave and millimeter-wave radar remote sensing, meta-materials, electromagnetic wave propagation, and antenna miniaturization. He has supervised 59 Ph.D. and numerous master's students and postdoctoral fellows. He together with his students were the recipient of 35 paper awards. He was a Member of NASA Advisory Council for two consecutive terms from 2006 to 2010 and the President of the IEEE Geoscience and Remote Sensing Society during 2015–2016. He is the past Chair of Commission F of USNC/URSI and is a Member of the AdCom for the IEEE Antennas and Propagation Society. He led the Center for Microelectronics and Sensors funded by Army Research Laboratory during 2008–2018 and is leading the Center of Excellence in Microwave Sensor Technology. His contributions to the field of electromagnetics have been recognized by many awards, including the Humboldt Research Award, IEEE GRSS Distinguished Achievement Award, IEEE Judith A. Resnik medal, IEEE GRSS Education Award, NASA Group Achievement Award, and many other wards from the University of Michigan. He is a Fellow of the American Association for the Advancement of Science, and Fellow of the National Academy of Inventors. He is a Member of the National Academy of Engineering.



John Soukar received the B.S. degree in microbiology from the University of Michigan, Ann Arbor, MI, USA, in 2019. He is currently working toward the Ph.D. degree in genetics and genomics with Texas A&M University, College Station, TX, USA. Since 2017, he has been a Technician with the Department of Emergency Laboratory and previously as an undergrad Research Assistant, under Dr. J. Scott VanEpps before beginning the Ph.D. degree in 2021. His research interests include inter- and intra-cellular interactions and nanomaterials.

Authorized licensed use limited to: The University of British Columbia Library. Downloaded on October 11,2026 at 00:43:51 UTC from IEEE Xplore. Restrictions apply.



Nicholas A. Kotov is Irving Langmuir Distinguished University Professor at the University of Michigan. He is a well-known pioneer of biomimetic nanostructures and self-assembled nanomaterials. He is heading now an international team of scientists working on practical implementations and theoretical foundations of biomimetic nanostructures. Chiral nanostructures represent a focal point in his current work with translation to physics, chemistry, biology, and medicine. Nicholas is a recipient of more than 50 awards and recognitions including ACS Award for Outstanding Achievements in Nanoscience (ACS), Newton Award (Department of Defense), MRS Medal (Materials Research Society), and UNESCO Medal for Development of Nanoscience and Nanotechnologies. Nicholas is a founder of seven startups that commercialized biomimetic nanostructures for energy, healthcare and automotive industry.



J. Scott VanEpps received the bachelor's degree in molecular biology and chemical engineering from the University of Pittsburgh, Pittsburgh, PA, USA, in 2001, and the M.D. and Ph.D. degrees in bioengineering from Medical Scientist Training Program, University of Pittsburgh, in 2009. He is currently an Assistant Professor with the Departments of Emergency Medicine and Biomedical Engineering, University of Michigan Ann Arbor, MI, USA. He is also a Faculty with the Biointerfaces Institute, Taubman Institute Emerging Scholar, and the Associate Director of the Max Henry Weil Institute for Critical Care Research and Innovation. He completed his residency in Emergency Medicine from the University of Michigan/St. Joseph Mercy Hospital in 2013 and joined the faculty with the University of Michigan. He is board certified in Emergency Medicine and sees patients in the Adult Emergency Department and the Emergency Critical Care Center, Michigan Medicine. He also runs a translational research laboratory focused on the development of novel diagnostic, treatment, and prevention strategies for life-threatening infections and in particular infections associated with medical device implants.

Authorized licensed use limited to: The University of British Columbia Library. Downloaded on October 11,2026 at 00:43:51 UTC from IEEE Xplore. Restrictions apply.